Characterization of single and colliding laser-produced plasma bubbles using Thomson scattering and proton radiography

M. J. Rosenberg,[1,*] J. S. Ross,[2] C. K. Li,[1] R. P. J. Town,[2] F. H. Séguin,[1] J. A. Frenje,[1] D. H. Froula,[3] and R. D. Petrasso[1]

[1]*Plasma Science and Fusion Center, Massachusetts Institute of Technology, Cambridge, Massachusetts 02139, USA*

[2]*Lawrence Livermore National Laboratory, Livermore, California 94550, USA*

[3]*Laboratory for Laser Energetics, University of Rochester, Rochester, New York 14623, USA*

(Received 17 September 2012; published 27 November 2012)

Time-resolved measurements of electron and ion temperatures using Thomson scattering have been combined with proton radiography data for comprehensive characterization of individual laser-produced plasma bubbles or the interaction of bubble pairs, where reconnection of azimuthal magnetic fields occurs. Measurements of ion and electron temperatures agree with LASNEX simulations of single plasma bubbles, which include the physics of magnetic fields. There is negligible difference in temperatures between a single plasma bubble and the interaction region of bubble pairs, although the ion temperature may be slightly higher due to the collision of expanding plasmas. These results are consistent with reconnection in a $\beta \sim 8$ plasma, where the release of magnetic energy (<5% of the electron thermal energy) does not appreciably affect the hydrodynamics.

DOI: 10.1103/PhysRevE.86.056407 PACS number(s): 52.50.Jm, 52.35.Vd, 52.38.Fz, 52.70.Kz

I. INTRODUCTION

Characterization of laser-produced plasmas is important in a variety of experiments relevant to both inertial confinement fusion and basic plasma physics, where measurements of the temperature and magnetic field evolution are critical to understanding the plasma dynamics [1–4]. Such plasmas are especially relevant in indirect-drive inertial confinement fusion, where multiple lasers irradiate the inside of a cylindrical hohlraum [5]. Previously, Thomson scattering [6] has been used to diagnose the temperature evolution of laser-produced plasmas, both in indirect-drive hohlraums [7] and in planar laser-foil experiments [8,9].

One particular scientific application of laser-foil interactions is the study of self-generated azimuthal magnetic fields around laser-produced, expanding, hemispherical plasma bubbles [10,11] and their reconnection. Magnetic reconnection [12] has been explored traditionally in the context of astrophysical plasmas [13,14] or in the laboratory with plasmas at low density ($\sim 10^{12}$–10^{14} cm^{-3}) and low plasma β, the ratio of thermal energy density to magnetic energy density ($\sim$0.001–0.1) [15–17]. Recent experiments have assessed the evolution and reconnnection of magnetic fields in the high-energy-density regime [18,19], through the interaction of multiple laser-produced plasma bubbles [9,20–23]. Several of these experiments have utilized the proton radiography technique [24] to probe these laser-produced plasma bubbles, producing quantitative data on the strength of laser-generated magnetic fields [9,20–22,25,26]. Although some measurements of electron and ion temperatures have been made in these experiments [9], there appears to be no published comprehensive, time-resolved set of measurements.

In this study, Thomson-scattering measurements have been used to characterize the temperature evolution at different times and locations in the laser-produced plasma bubbles and in the interaction region of bubble pairs. The data offer a comprehensive, time-resolved set of measurements of local electron and ion temperatures in single and interacting laser-produced plasma bubbles, in conjunction with proton radiography data used to infer magnetic fields. Measurements of electron and ion temperatures in the reconnection region of laser-generated magnetic fields provide unique information on the temperature evolution in a high-β reconnection event. By juxtaposing temperature data in the reconnection region to comparable data in the single-bubble experiment, it is possible to infer the role of magnetic reconnection and the hydrodynamic collision of the two bubbles in shaping the thermal properties of the plasma.

This paper is organized as follows: Sec. II describes the experiments and measurement techniques; Sec. III contrasts experimental and modeled results; Sec. IV discusses the findings; and Sec. V presents concluding remarks.

II. EXPERIMENTS

Laser-foil experiments were conducted at the OMEGA laser facility [27]. In each experiment, a 5-μm CH foil was irradiated by one or two 351-nm (3ω) beams in a 1-ns pulse with 500 J/beam and phase plates that produce an 800-μm spot size with a fourth-order super-Gaussian profile [28]. For the dual-beam reconnection experiments, laser spots were separated by 1.2–1.4 mm. In separate experiments, monoenergetic proton radiography data [29] and 4ω Thomson-scattering data [30] were obtained for the single or pair of laser-foil interactions. These experiments provide complementary information on the evolution of magnetic fields and ion and electron temperatures both in laser-produced plasma bubbles and in the magnetic reconnection of bubble pairs.

The setup for the Thomson-scattering experiments is shown in Fig. 1. The Thomson-scattering technique utilizes a frequency-quadrupled (263.5-nm) probe beam and a streaked detector system for time-resolved measurements of the scattered light spectrum, from which electron and ion temperature histories are inferred for the laser-produced plasma [30]. On different shots, the probe beam was focused onto three different locations in each of the [Fig. 1(b)] single-bubble

*mrosenbe@mit.edu

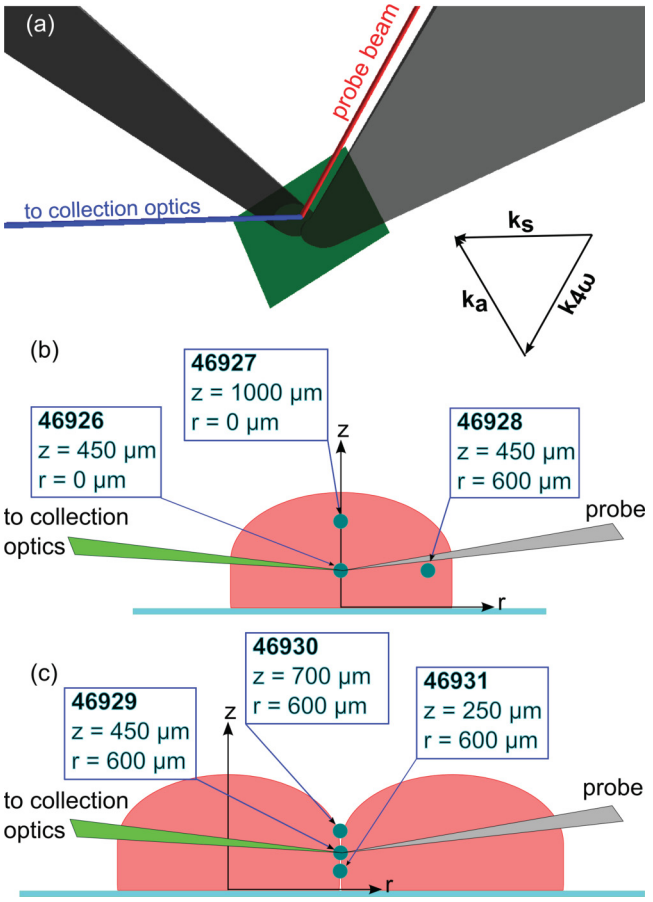

FIG. 1. (Color online) Experimental setup for the Thomson-scattering experiments (a). In these experiments, the Thomson-scattering probe beam was incident at a 79° angle relative to the foil normal (z axis), nearly parallel to the foil surface, while the detector was at 37° to the normal, such that the scattering angle was 63° and the scattering vector 21° to the foil normal. Locations probed are shown for (b) single-bubble experiments and (c) reconnection experiments.

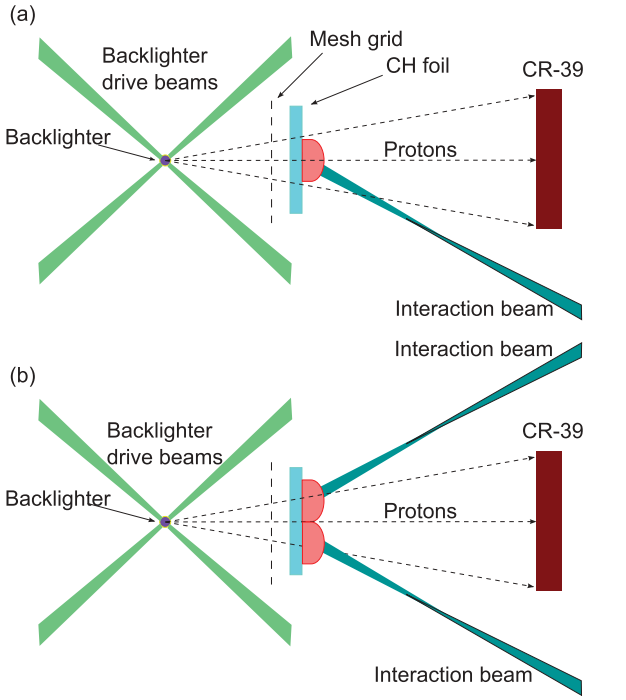

FIG. 2. (Color online) Proton radiography setup for (a) the single-bubble experiments and (b) the reconnection experiments. The distance between the backlighter and the CH foil is 15 mm, while the distance between the mesh grid and the foil is 2 mm. These experiments, the first using this configuration, were originally reported by Li *et al.* [20,25].

and [Fig. 1(c)] interacting-bubble geometry. The Thomson-scattering volume can be described as a cylinder approximately 60 μm in diameter and ~75 μm in length, providing a local measurement of the plasma conditions [30].

From the spectrum of light scattered by ion-acoustic fluctuations the electron and ion temperatures can be determined [6]. To first order, the electron temperature is proportional to the square of the wavelength shift of the probe beam; the spectral shape of ion-acoustic features is sensitive also to the ion temperature [7]. The electron density can also be inferred from the absolute magnitude of the scattered light spectrum, but density measurements were not obtained in this study.

The proton radiography setup is shown in Fig. 2 for both (a) the single-laser-foil experiments and (b) the dual-laser-foil (reconnection) experiments. A D^3He-filled, thin-glass-shell backlighter was illuminated by 20 OMEGA beams, delivering 8.5 kJ in a 1-ns pulse and producing monoenergetic 3- and 15-MeV protons from respective DD and D^3He fusion reactions. These backlighter protons were divided by a mesh grid into discrete beamlets before sampling the laser-produced CH plasma. The proton beamlets were then deflected by magnetic fields surrounding the plasma bubbles and their positions were recorded using the solid-state nuclear track detector CR-39. Given the known proton energy as measured by proton spectrometers [31], the measured deflection of each beamlet was used to infer quantitatively the path-integrated magnetic field strength through the plasma. The absolute timing of the proton arrival at the plasma was determined by the proton temporal diagnostic (PTD) [32], which measures the time of proton emission from the backlighter. These experiments were described originally by Li *et al.* for single laser-produced plasma bubbles [25] and for the interaction of multiple bubbles [20]. Although the Thomson-scattering measurements and the proton radiography data were obtained on different shots, the experiments used comparable laser and target parameters.

III. RESULTS

Images of both individual and interacting plasma bubbles, using 15-MeV protons, are shown in Fig. 3. These images, which have been published previously, reveal the evolution and reconnection of magnetic fields around laser-produced plasma bubbles [20,25]. The published images are used here to illustrate the location of Thomson-scattering regions in the nearly identical experiments conducted in this work. In the single-bubble images [Fig. 3(a)], Thomson-scattering regions are located either at the center of the bubble (red star, $r = 0$, $z = 450$ and 1000 μm) or towards the bubble edge (green

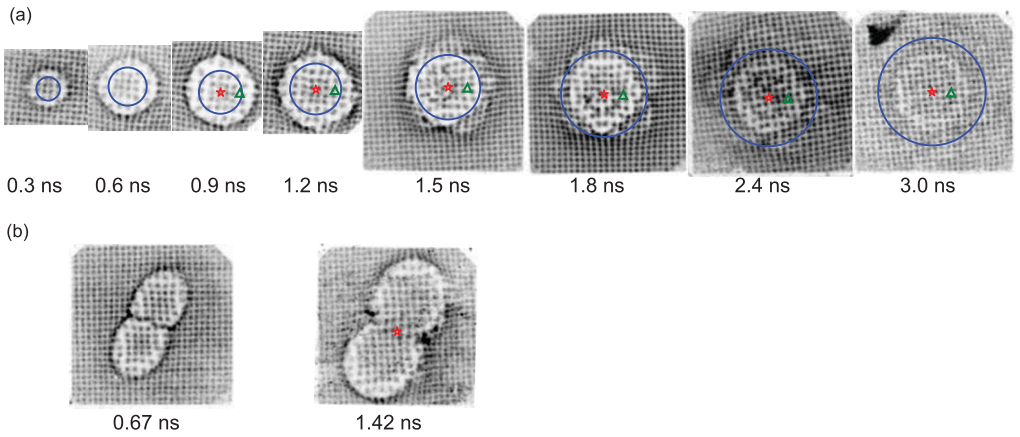

FIG. 3. (Color online) 15-MeV-proton radiography images of (a) single laser-produced plasma bubbles and (b) interacting plasma bubbles undergoing magnetic reconnection. The approximate bubble size is indicated in the single-bubble images (blue circle), and the locations of Thomson-scattering regions are shown at $r = 0$ (red star, for both $z = 450$ μm and $z = 1000$ μm) and at $r = 600$ μm (green triangle, for $z = 450$ μm) for $t > 0.9$ ns. In the interacting-bubbles experiments, the Thomson-scattering regions are located in the reconnection layer at $r = 600$ μm (red star, for $z = 250$ μm, $z = 450$ μm, and $z = 700$ μm). These images were first published by Li *et al.* [20,25].

triangle, $r = 600$ μm, $z = 450$ μm). The approximate bubble size (blue circle) is shown to illustrate the location of the bubble perimeter relative to the outer Thomson-scattering region. Note that the bubble edge is not the location of beamlet pileup, since that feature is the result of proton deflection and does not represent the actual radius of the bubble. The sample times indicated for the proton radiography images were obtained using the PTD. Since the bubble has expanded beyond a radius of 600 μm by $t = 0.9$ ns, the Thomson-scattering data at $r = 600$ μm obtained for $t > 0.9$ ns are well within the bubble perimeter.

Thomson-scattering measurements in the reconnection experiments [Fig. 3(b)] were all made in the center of the reconnection region, at the midpoint between the bubble centers (red star, at $z = 250$, 450, and 700 μm). As shown in the first reconnection image, the interaction of the two plasma bubbles has already begun at $t = 0.67$ ns. Thomson-scattering measurements of the interacting plasma bubbles were made from $t \sim 0.8$–3.1 ns, so the data are obtained when the bubbles are interacting and their magnetic fields reconnecting.

Streaked Thomson-scattering spectra are shown in Fig. 4, for each of the experimental geometries depicted in Fig. 1.

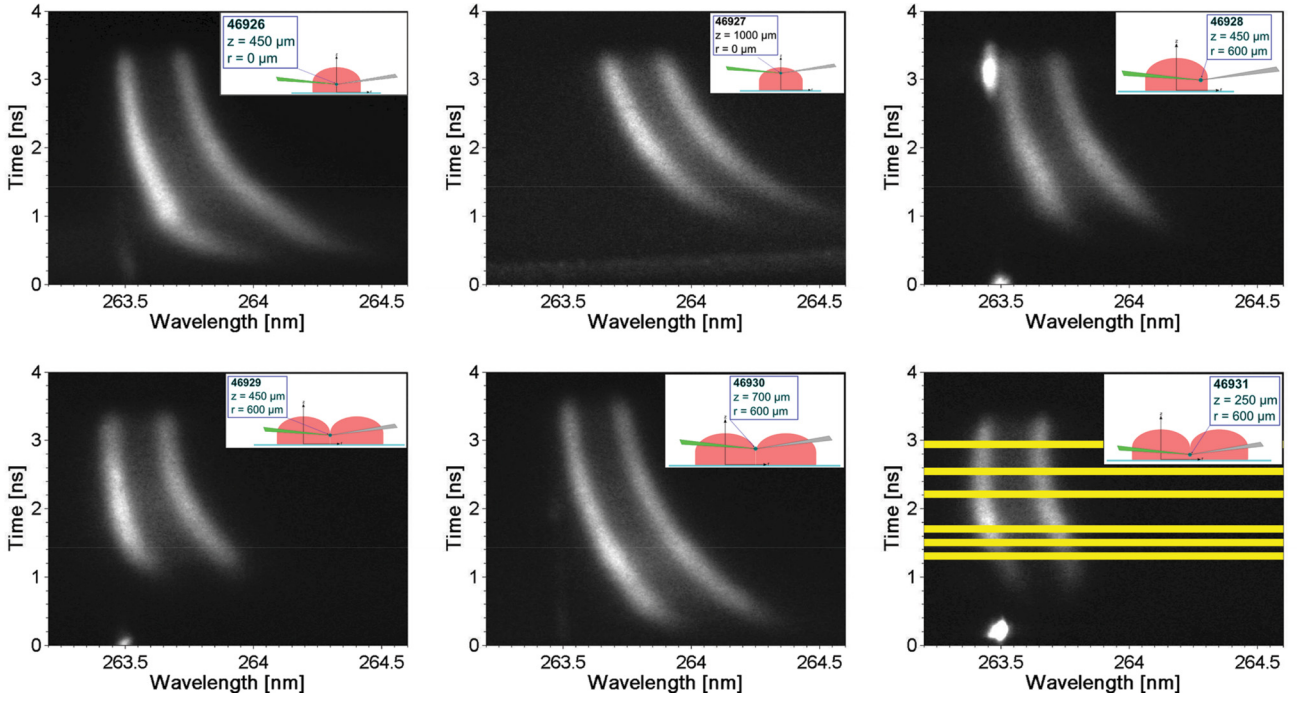

FIG. 4. (Color online) Streaked Thomson-scattering spectra from single-bubble experiments (top) and interacting-bubble experiments (bottom), at the locations depicted in Fig. 1. The horizontal yellow bars in the bottom right image indicate the times that were chosen for spectral analysis for shot 46931. For improved statistics, the spectra were integrated over 120 ps at each lineout, as indicated by the width of the bars. The resulting lineouts are shown in Fig. 5.

These images show the time evolution of scattered light spectra and reflect changes in the plasma conditions at the particular locations in the experiments. Wavelength shifts in both features reflect changes in the plasma flow, while changes in the interline spacing indicate evolution of the electron temperature [6]. Lineouts are taken to produce spectra at different times throughout the experiment from which the time history of electron and ion temperatures is inferred.

The times chosen for spectral analysis in shot 46931 are shown at the bottom right of Fig. 4. Each lineout integrates over 120 ps to reduce the statistical noise in the spectrum. The relative timing of the spectral snapshots within a particular shot is known to ± 50 ps, while the absolute uncertainty in the timing is ± 100 ps. The resulting spectra and their fits are shown in Fig. 5. The fitted spectra are convolutions of the Thomson-scattering form factor and the estimated instrumental response function, represented by a Gaussian of full width at half maximum 0.055 nm. Additional broadening of the measured spectral features not accounted for by the fits may be due to spatial gradients of electron and ion temperatures across the finite Thomson-scattering volume. Uncertainties in the inferred electron and ion temperatures are based on the quality of fit.

Measurements of the time-dependent electron and ion temperatures at three locations in the single-bubble plasma are shown on the left side of Fig. 6 and compared to temperatures predicted by two-dimensional (2D) LASNEX [33] hydrodynamics simulations at the appropriate location. The LASNEX simulations used in this study include the physics of magnetic fields and their generation from nonparallel gradients in electron temperature and electron density [34,35]. The simulations include flux-limited electron diffusion and the Braginskii cross-field transport terms, which may modify hydrodynamic profiles [36]. The inclusion of magnetic fields has little effect ($<10\%$) on LASNEX predictions of electron and ion temperatures over the time when Thomson-scattering measurements were obtained.

The overall electron temperature behavior agrees with the LASNEX simulations. The electron temperature at each location decreases after the laser turns off around $t \sim 1$ ns, with the magnitude and time scale of decay generally matching those predicted by LASNEX over the period $1 < t < 2$ ns. Beyond $t \sim 2$ ns, the measured electron temperatures level off around 300 eV, while the simulated electron temperatures continue to decrease. This discrepancy may be caused by slight heating of the plasma by the probe beam at late times, which is not accounted for in the LASNEX simulations. At $t \sim 1.5$ ns, the measured electron temperatures appear slightly lower than LASNEX predictions. Such a discrepancy would be consistent with the previous observation of magnetic fields around a single plasma bubble decaying faster than predicted [25]. That result could be explained by the measured electron temperature being lower than the simulated temperature, which would produce a faster diffusion of magnetic fields.

The ion temperature measurements also agree with the LASNEX simulations. In some experiments, the early-time ion temperatures are higher than predicted, although there is a large uncertainty in those measurements due to relatively poor fits to the measured spectrum. As the ion temperature is inferred from the ratio of trough to peak amplitude in the scattered light spectrum, its uncertainty is especially sensitive to the looseness of fit caused by temperature gradients across the Thomson-scattering volume. In all three single-bubble experiments at $t > 1.5$ ns, the timing of the ion temperature evolution matches LASNEX predictions, consistent with what was observed for the electron temperatures.

Thomson-scattering measurements of electron and ion temperatures in the reconnection region of the colliding plasma

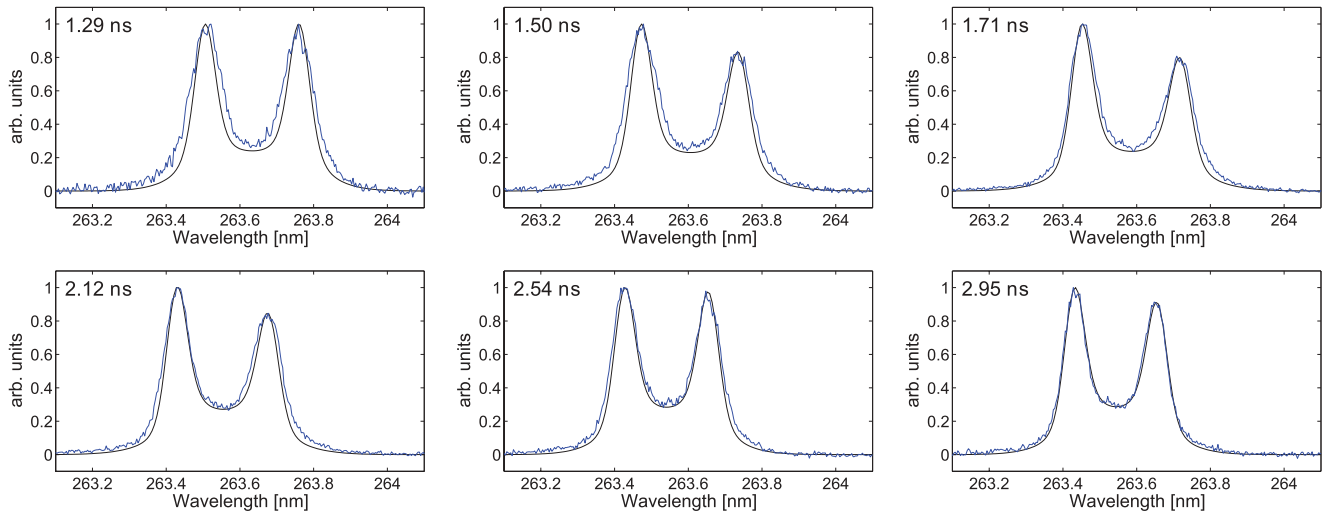

FIG. 5. (Color online) Measured spectra (jagged blue curves) and their fits (smooth black curves) obtained from six lineouts of the streaked image on shot 46931 shown in Fig. 4. Changes in the interline spacing and the ratio of trough to peak amplitude depict evolution of the electron and ion temperatures at ($r = 600$ μm, $z = 250$ μm) in the interaction region of the colliding plasmas. Additional broadening of measured spectral features in comparison to their fits may be due to spatial gradients in electron and ion temperatures across the Thomson-scattering volume.

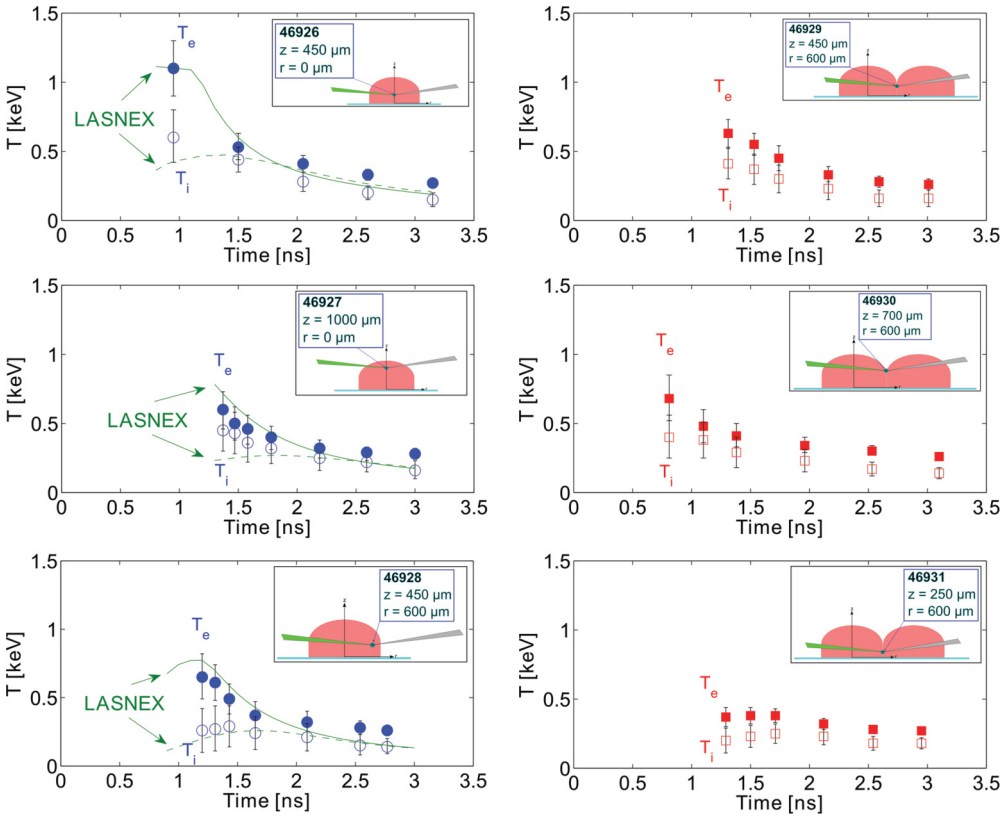

FIG. 6. (Color online) Simultaneous, time-dependent Thomson-scattering measurements of electron temperatures (filled markers) and ion temperatures (open markers) at different positions in the single bubble (left) and interacting bubbles (right). Single-bubble data are compared to LASNEX predictions of electron temperatures (solid lines) and ion temperatures (dashed lines). Comparisons between measured electron and ion temperatures demonstrate differences in electron-ion thermal equilibration at different locations and times in these experiments, as discussed in Sec. IV.

bubbles are shown on the right side of Fig. 6. At each height in the reconnection layer, the electron temperature decreases after the laser has turned off. At $z = 450$ μm and $z = 700$ μm, the ion temperature decreases monotonically, while at $z = 250$ μm, there is a slight increase in the ion temperature for $1 < t < 1.7$ ns before it decreases. Since the interacting plasma bubbles are inherently three dimensional, 2D LASNEX simulations are not applicable for these experiments.

IV. DISCUSSION

The single-bubble electron and ion temperature data are well modeled by LASNEX and depict the convection and cooling of the laser-produced plasma bubble in the period after laser shutoff, as the bubble is allowed to expand into the ambient vacuum. Measured electron and ion temperatures at fixed points in the experimental geometry level off at late times, as hotter plasma near the bubble center is convected through the Thomson-scattering regions. At all three locations in the single plasma bubble, the measured electron temperature at $t > 2$ ns is greater than the LASNEX predictions, possibly due to continued heating of the plasma by the Thomson-scattering probe beam. It should be noted that the late-time comparison of experimental data to LASNEX simulations is complicated also by the emergence of instabilities, which break the 2D bubble symmetry after the laser turns off around $t \sim 1.2$ ns [25].

Having measurements of the conditions in both single and interacting plasma bubbles allows assessment of the effect of the plasma collision and magnetic reconnection on the energetics of the system. A comparison of time-dependent electron and ion temperatures measured at ($r = 600$ μm, $z = 450$ μm) in the single-bubble case versus the interacting-bubble case is shown in Fig. 7. As shown in Fig. 7(a), there is a negligible difference in the electron temperature history between the single bubble and reconnection cases during the time when magnetic reconnection is occurring between the two bubbles. Thus, the magnetic field energy released during reconnection does not noticeably raise the electron temperature. This result is in contrast to the findings of Nilson *et al.* [9], where an increase in the electron temperature to 1.7 keV was inferred from Thomson-scattering measurements in the reconnection region of laser-produced plasma bubbles. The minimal impact of magnetic reconnection on the electron temperature of the plasma is expected for reconnection at high plasma β, where the magnetic pressure is small in comparison to the hydrodynamic pressure of the plasma.

The ion temperature histories [Fig. 7(b)] are nearly identical given the large uncertainties at early times, although the appearance of a slightly higher T_i in the colliding-bubble case at $t \sim 1.3$ ns is suggestive of a hydrodynamic collision

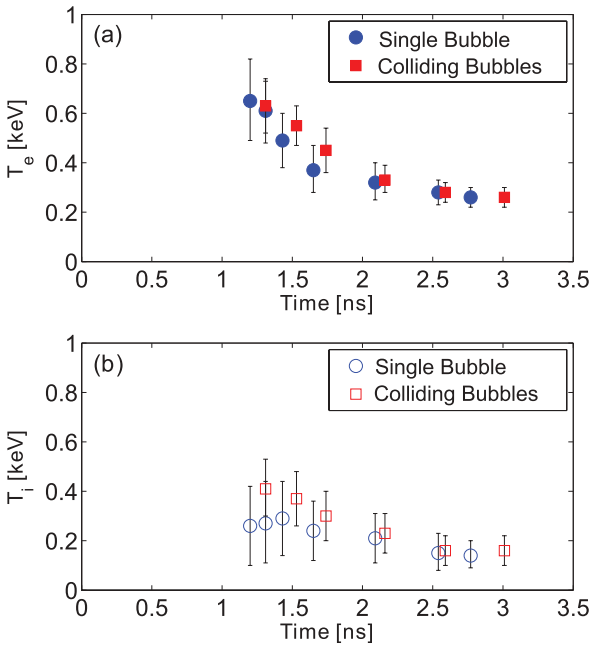

FIG. 7. (Color online) Comparison of time-dependent (a) electron temperature and (b) ion temperature for single plasma bubbles (blue circles) and colliding plasma bubbles (red squares) after the bubble collision around $t \sim 0.7$ ns. There is a negligible difference in temperatures between the single-bubble and colliding-bubble cases, although the ion temperature around $t = 1.3$ ns is ~50% higher in the colliding-bubble case (barely within the uncertainty). These results are consistent with the hydrodynamic collision of plasma bubbles at $\beta \gg 1$.

of plasmas, independent of magnetic reconnection [37]. The ion-ion mean free path under these conditions is approximately 1 μm, so the plasma is collisional and some kinetic energy from the colliding plasmas is expected to be transferred to ion thermal energy.

These data can also be used to more precisely identify the plasma β for these laser-produced plasmas, defined as

$$\beta = \frac{n_i k T_i + n_e k T_e}{B^2/2\mu_0}, \tag{1}$$

where n_i (n_e) and T_i (T_e) are the ion (electron) density and temperature, and B is the magnetic field strength. LASNEX simulations give an approximate electron density, while Thomson-scattering and proton radiography data give the temperatures and the magnetic field strength, respectively. Since each of the measurements is performed locally and at different times, care must be taken to ensure that appropriate values are used. For example, proton radiography data provide snapshots of the magnetic field strength at the expanding bubble perimeter where the magnetic fields are concentrated, while Thomson-scattering data are taken at fixed locations (e.g., $r = 600$ μm).

At $t = 0.91$ ns in the single-bubble experiment, the bubble perimeter is located at $r = 700$ μm, just outside the Thomson-scattering region at $r = 600$ μm. At $t = 1.20$ ns, the earliest Thomson-scattering measurement at that location gives $T_e = 0.65$ keV and $T_i = 0.26$ keV at ($r = 600$ μm, $z = 450$ μm). These temperatures, and the ~0.5 MG magnetic field inferred from the proton radiography data, are approximately representative of the plasma conditions at the bubble perimeter at $t = 0.9$–1.2 ns and $r = 600$–700 μm. Along with the LASNEX-predicted electron density of 7×10^{19} cm^{-3}, these parameters are used to estimate $\beta \sim 8$. Therefore, the magnetic energy density is approximately one-eighth of the total thermal energy density at the bubble perimeter.

Similarly, the expansion velocity of the plasma bubble can be used to infer the ratio of plasma thermal energy to kinetic energy of the expanding plasma bubble. For a bubble expansion velocity of $V \sim 500$ μm/ns, as inferred from proton radiography data [25] and consistent with the Doppler shifts in the Thomson-scattering spectra, there is approximately three times as much energy contained in the kinetic energy of the expanding bubble ($\frac{1}{2} n_i m_i V^2$) as there is contained in the thermal energy ($n_i k T_i + n_e k T_e$), and about 25 times as much energy as in the magnetic fields ($B^2/2\mu_0$). These results reinforce the picture of plasma bubble interaction where the dynamics is dominated by hydrodynamic processes, even though energy is released by the reconnection of large magnetic fields. At the high densities present in these experiments, the maximum energy released by the dissipation of 0.5-MG magnetic fields sets an upper bound on the increase in electron temperature of ~80 eV. The actual energy released is estimated to be lower [20], corresponding to an electron temperature increase of only ~20 eV. Each of these estimates is negligible compared to the measured electron temperature of 650 eV.

The conditions under which magnetic reconnection occurs can be further specified by comparing time scales of different physical processes in the plasma bubbles prior to their collision. The magnetic Reynolds number (Rm), the ratio of resistive to flow time scales, is ~2000, affirming that advection is the dominant mechanism in transporting the magnetic fields to the reconnection layer. Under such conditions, stretching of magnetic field lines [38] and pileup of magnetic flux may occur, as is predicted in colliding plasma bubbles [23]. However, the Thomson-scattering data indicate that even if the magnetic field strength is enhanced locally, the release of magnetic energy is insufficient to appreciably increase the electron temperature. The Lundquist number (S), the ratio of resistive to Alfvén crossing times, is ~400 for this reconnection event, small enough to produce a fairly stable reconnection.

The simultaneous, time-resolved measurements of electron and ion temperatures shown in Fig. 6 hint at the process of thermal equilibration between species at different locations in the expanding plasma bubble. It should be emphasized that these time-dependent measurements are not tracking a parcel of plasma, but rather sampling different locations in the bubble geometry as they pass through the fixed Thomson-scattering region (e.g., at $r = 600$ μm, $z = 450$ μm).

In the single-bubble case, at each of ($r = 0$, $z = 450$ μm), ($r = 0$, $z = 1000$ μm), and ($r = 600$ μm, $z = 450$ μm), the electron temperature is greater than the ion temperature at $t \sim 1.2$ ns by a factor of ~1.5–2.5, due to the preferential absorption of laser light by the electrons. As the central region of the plasma bubble expands through the Thomson-scattering regions, the electrons and ions move closer to equilibrium, such

that by $t \sim 1.8$ ns, the temperatures are within 25% of each other. The difference between electron and ion temperatures in the colliding-bubbles experiments is not substantially different from that in the single-bubble case, and temperatures approach each other gradually for $t > 1$ ns. In both sets of experiments, the electron and ion temperatures never quite equilibrate. This result may be due to the absorption of energy from the Thomson-scattering probe beam, which preferentially heats the electrons.

For a CH plasma at $n_e \sim 10^{20}$ cm^{-3} and $T_e \sim 650$ eV, conditions near the bubble perimeter ($r = 600$ μm, $z = 450$ μm) at early times, the electron-ion equilibration time is $\tau_{eq} \sim 4$ ns. As this time scale is longer than the duration of the experiment, it is unlikely that the perimeter plasma experiences significant thermal equilibration. The appearance of equilibration is more likely a consequence of the convection of plasma from denser regions at the center of the bubble, where an electron density of $\sim 5 \times 10^{20}$ cm^{-3} is predicted at early times. The equilibration time under those conditions is closer to $\tau_{eq} \sim 1$ ns, so some thermal equilibration likely has occurred by the time that plasma passes through the Thomson-scattering region.

V. CONCLUSIONS

Time-resolved electron and ion temperature data have been presented for single and colliding plasma bubbles generated by laser-foil interactions. These data have been combined with magnetic field data to produce a comprehensive picture of the thermal and magnetic evolution of both individual plasma bubbles and the magnetic reconnection of interacting bubble pairs. The single-bubble electron and ion temperature data are in good agreement with LASNEX simulations.

Comparison of the temperature data between the single bubble and the interacting bubbles elucidates the impact of magnetic reconnection and hydrodynamic collision on the thermal properties of the plasma. The temperature data reveal a negligible difference between the single bubble and the reconnection case, although the ion temperature may be slightly higher at early times in the bubble collision. These results are consistent with the hydrodynamic collision of plasma bubbles at $\beta \gg 1$, where magnetic reconnection does not appreciably alter the dynamics, and the estimated increase in electron temperature due to the release of magnetic energy is <5% of the total. A comparison of the energy sources in the system corroborates this picture: the kinetic energy density of the expanding bubble is ~3 times its thermal energy density and ~25 times its magnetic energy density. These data will help guide future studies of magnetic reconnection and basic plasma physics using laser-foil interactions.

ACKNOWLEDGMENTS

The authors thank the OMEGA operations crew for their assistance in carrying out these experiments. This work is supported in part by US DOE (Grant No. DE-FG52-09NA29553), NLUF (Grant No. DE-NA0000877), LLE (Grant No. 414-090-G), and LLNL (Grant No. B580243).

[1] P. K. Carroll and E. T. Kennedy, Contemp. Phys. **22**, 61 (1981).
[2] P. T. Rumsby and J. W. M. Paul, Phys. Plasmas **16**, 247 (1974).
[3] J. A. Stamper and B. H. Ripin, Phys. Rev. Lett. **34**, 138 (1975).
[4] S. P. Regan, D. K. Bradley, A. V. Chirokikh, R. S. Craxton, D. D. Meyerhofer, W. Seka, R. W. Short, A. Simon, R. P. J. Town, B. Yaakobi, J. J. Carroll III, and R. P. Drake, Phys. Plasmas **6**, 2072 (1999).
[5] J. Lindl, Phys. Plasmas **2**, 3933 (1995).
[6] D. H. Froula, S. H. Glenzer, J. N. C. Luhmann, and J. Sheffield, *Plasma Scattering of Electromagnetic Radiation*, 2nd ed. (Academic Press, Burlington, MA, 2011).
[7] D. H. Froula, J. S. Ross, L. Divol, N. Meezan, A. J. MacKinnon, R. Wallace, and S. H. Glenzer, Phys. Plasmas **13**, 052704 (2006).
[8] S. H. Glenzer, W. E. Alley, K. G. Estabrook, J. S. D. Groot, M. G. Haines, J. H. Hammer, J.-P. Jadaud, B. J. MacGowan, J. D. Moody, W. Rozmus, L. J. Suter, T. L. Weiland, and E. A. Williams, Phys. Plasmas **6**, 2117 (1999).
[9] P. M. Nilson, L. Willingale, M. C. Kaluza, C. Kamperidis, S. Minardi, M. S. Wei, P. Fernandes, M. Notley, S. Bandyopadhyay, M. Sherlock, R. J. Kingham, M. Tatarakis, Z. Najmudin, W. Rozmus, R. G. Evans, M. G. Haines, A. E. Dangor, and K. Krushelnick, Phys. Rev. Lett. **97**, 255001 (2006).
[10] J. A. Stamper, K. Papadopoulos, R. N. Sudan, S. O. Dean, and E. A. McLean, Phys. Rev. Lett. **26**, 1012 (1971).
[11] M. G. Haines, Phys. Rev. Lett. **78**, 254 (1997).
[12] D. Biskamp, *Magnetic Reconnection in Plasmas* (Cambridge University Press, Cambridge, UK, 2000).
[13] S. Tsuneta, Astrophys. J. **456**, 840 (1996).
[14] B. U. O. Sonnerup, G. Paschmann, I. Papamastorakis, N. Sckopke, G. Haerendel, S. J. Bame, J. R. Asbridge, J. T. Gosling, and C. T. Russell, J. Geophys. Res. **86**, 10049 (1981).
[15] J. Egedal, W. Fox, N. Katz, M. Porkolab, K. Reim, and E. Zhang, Phys. Rev. Lett. **98**, 015003 (2007).
[16] H. Ji, M. Yamada, S. Hsu, and R. Kulsrud, Phys. Rev. Lett. **80**, 3256 (1998).
[17] In astrophysical plasmas, the regimes in which reconnection takes place can vary quite substantially. Electron densities range from 10^{-1} cm^{-3} in the Earth's magnetotail to 10^{11} cm^{-3} in the solar chromosphere, while plasma β values range from $\sim 10^{-4}$ in the solar corona to ~1 at the Earth's magnetopause to ~100 in the solar photosphere.
[18] R. C. Davidson, *Frontiers in High Energy Density Physics* (National Academies Press, Washington, DC, 2003).
[19] R. P. Drake, *High-Energy-Density Physics* (Springer Press, New York, 2006).
[20] C. K. Li, F. H. Séguin, J. A. Frenje, J. R. Rygg, R. D. Petrasso, R. P. J. Town, O. L. Landen, J. P. Knauer, and V. A. Smalyuk, Phys. Rev. Lett. **99**, 055001 (2007).
[21] P. M. Nilson, L. Willingale, M. C. Kaluza, S. Minardi, M. S. Wei, P. Fernandes, M. Notley, S. Bandyopadhyay, M. Sherlock, R. J. Kingham, M. Tatarakis, Z. Najmudin, W. Rozmus, R. G. Evans, M. G. Haines, A. E. Dangor, and K. Krushelnick, Phys. Plasmas **15**, 092701 (2008).

[22] L. Willingale, P. M. Nilson, M. C. Kaluza, A. E. Dangor, R. G. Evans, P. Fernandes, M. G. Haines, C. Kamperidis, R. J. Kingham, C. P. Ridgers, M. Sherlock, A. G. R. Thomas, M. S. Wei, Z. Najmudin, K. Krushelnick, S. Bandyopadhyay, M. Notley, S. Minardi, M. Tatarakis, and W. Rozmus, Phys. Plasmas **17**, 043104 (2010).

[23] W. Fox, A. Bhattacharjee, and K. Germaschewski, Phys. Rev. Lett. **106**, 215003 (2011).

[24] A. J. Mackinnon, P. K. Patel, R. P. Town, M. J. Edwards, T. Phillips, S. C. Lerner, D. W. Price, D. Hicks, M. H. Key, S. Hatchett, S. C. Wilks, M. Borghesi, L. Romagnani, S. Kar, T. Toncian, G. Pretzler, O. Willi, M. Koenig, E. Martinolli, S. Lepape, A. Benuzzi-Mounaix, P. Audebert, J. C. Gauthier, J. King, R. Snavely, R. R. Freeman, and T. Boehly, Rev. Sci. Instrum. **75**, 3531 (2004).

[25] C. K. Li, F. H. Séguin, J. A. Frenje, J. R. Rygg, R. D. Petrasso, R. P. J. Town, P. A. Amendt, S. P. Hatchett, O. L. Landen, A. J. Mackinnon, P. K. Patel, M. Tabak, J. P. Knauer, T. C. Sangster, and V. A. Smalyuk, Phys. Rev. Lett. **99**, 015001 (2007).

[26] R. D. Petrasso, C. K. Li, F. H. Seguin, J. R. Rygg, J. A. Frenje, R. Betti, J. P. Knauer, D. D. Meyerhofer, P. A. Amendt, D. H. Froula, O. L. Landen, P. K. Patel, J. S. Ross, and R. P. J. Town, Phys. Rev. Lett. **103**, 085001 (2009).

[27] T. R. Boehly, D. L. Brown, R. S. Craxton, R. L. Keck, J. P. Knauer, J. H. Kelly, T. J. Kessler, S. A. Kumpan, S. J. Loucks, S. A. Letzring, F. J. Marshall, R. L. McCrory, S. F. B. Morse, W. Seka, J. M. Soures, and C. P. Verdon, Opt. Commun. **133**, 495 (1997).

[28] H. T. Powell and T. J. Kessler, *Laser Coherence Control: Technology and Applications* (Society of Photo-optical Instrumentation Engineers, Bellingham, WA, 1993).

[29] C. K. Li, F. H. Séguin, J. A. Frenje, J. R. Rygg, R. D. Petrasso, R. P. J. Town, P. A. Amendt, S. P. Hatchett, O. L. Landen, A. J. Mackinnon, P. K. Patel, V. A. Smalyuk, T. C. Sangster, and J. P. Knauer, Phys. Rev. Lett. **97**, 135003 (2006).

[30] D. H. Froula, J. S. Ross, L. Divol, and S. H. Glenzer, Rev. Sci. Instrum. **77**, 10E522 (2006).

[31] F. H. Séguin, J. A. Frenje, C. K. Li, D. G. Hicks, S. Kurebayashi, J. R. Rygg, B. E. Schwartz, R. D. Petrasso, S. Roberts, J. M. Soures, D. D. Meyerhofer, T. C. Sangster, J. P. Knauer, C. Sorce, V. Y. Glebov, C. Stoeckl, T. W. Phillips, R. J. Leeper, K. Fletcher, and S. Padalino, Rev. Sci. Instrum. **74**, 975 (2003).

[32] J. A. Frenje, C. K. Li, F. H. Séguin, J. Deciantis, S. Kurebayashi, J. R. Rygg, R. D. Petrasso, J. Delettrez, V. Y. Glebov, C. Stoeckl, F. J. Marshall, D. D. Meyerhofer, T. C. Sangster, V. A. Smalyuk, and J. M. Soures, Phys. Plasmas **11**, 2798 (2004).

[33] G. B. Zimmerman and W. L. Kreur, Comments Plasma Phys. Controlled Fusion **2**, 51 (1975).

[34] P. D. Nielsen and G. B. Zimmerman, Lawrence Livermore National Laboratory Report No. UCRL-53123, 1981 (unpublished).

[35] R. P. J. Town *et al.*, Bull. Am. Phys. Soc. **50**, 123 (2005).

[36] J. A. Harte, W. E. Alley, D. S. Bailey, J. L. Eddleman, and G. B. Zimmerman, Lawrence Livermore National Laboratory Report No. UCRL-LR-105821-96-4, 1996 (unpublished), p. 150.

[37] O. Rancu, P. Renaudin, C. Chenais-Popovics, H. Kawagoshi, J. C. Gauthier, M. Dirksmoller, T. Missalla, I. Uschmann, E. Forster, O. Larroche, O. Peyrusse, O. Renner, E. Krouský, H. Pépin, and T. Shepard, Phys. Rev. Lett. **75**, 3854 (1995).

[38] G. Gregori, F. Miniati, D. Ryu, and T. W. Jones, Astrophys. J. **543**, 775 (2000).